Low-momentum-transfer nonrelativistic limit of the relativistic impulse approximation expression for Compton-scattering doubly differential cross sections and characterization of their relativistic contributions

L. A. LaJohn

Department of Physics and Astronomy, University of Pittsburgh, Pittsburgh, Pennsylvania 15260, USA

(Received 13 July 2009; revised manuscript received 8 January 2010; published 12 April 2010)

The nonrelativistic (nr) impulse approximation (NRIA) expression for Compton-scattering doubly differential cross sections (DDCS) for inelastic photon scattering is recovered from the corresponding relativistic expression (RIA) of Ribberfors [Phys. Rev. B **12**, 2067 (1975)] in the limit of low momentum transfer ($q \to 0$), valid even at relativistic incident photon energies $\omega_1 > m$ provided that the average initial momentum of the ejected electron $\langle p_i \rangle$ is not too high, that is, $\langle p_i \rangle < m$. This corresponds to a binding energy $E_b < 10$ keV. This $q \to 0$ nr limit is simultaneous with the approach of the scattering angle θ to 0° ($\theta \to 0^\circ$) around the Compton peak maximum. This explains the observation that it is possible to obtain an accurate Compton peak (CP) even when $\omega_1 > m$ using nr expressions when θ is small. For example, a 1% accuracy can be obtained when $\omega_1 = 1$ MeV if $\theta < 20^\circ$. However as ω_1 increases into the MeV range, the maximum θ at which an accurate Compton peak can be obtained from nr expressions approaches closer to zero, because the θ at which the relativistic shift of CP to higher energy is greatest, which starts at 180° when $\omega_1 < 300$ keV, begins to decrease, approaching zero even though the θ at which the relativistic increase in the CP magnitude remains greatest around $\theta = 180^\circ$. The relativistic contribution to the prediction of Compton doubly differential cross sections (DDCS) is characterized in simple terms using Ribberfors further approximation to his full RIA expression. This factorable form is given by DDCS $= KJ$, where K is the kinematic factor and J the Compton profile. This form makes it possible to account for the relativistic shift of CP to higher energy and the increase in the CP magnitude as being due to the dependence of $J(p_{\min}, \rho_{\rm rel})$ (where $p_{\min}$ is the relativistic version of the z component of the momentum of the initial electron and $\rho_{\rm rel}$ is the relativistic charge density) and $K(p_{\min})$ on $p_{\min}$. This characterization approach was used as a guide for making the nr QED S-matrix expression for the Compton peak kinematically relativistic. Such modified nr expressions can be more readily applied to large systems than the fully relativistic version.

DOI: 10.1103/PhysRevA.81.043404 PACS number(s): 32.80.Aa

I. INTRODUCTION

The main purpose for this work is to show that there is a low-momentum-transfer (q) nonrelativistic (nr) limit for the relativistic impulse approximation (RIA) expression for Compton doubly differential cross sections (DDCS) (differential with respect to the energy and angle of the scattered photon with the ejected electron not observed) and that one can recover the corresponding nr expressions, then to use this $q \to 0$ nr limit as a basis for characterizing relativistic contributions to the Compton peak. This provides an explanation for why it is possible to obtain an accurate Compton peak even at relativistic photon energies if the scattering angle is small. Another purpose is to show that this characterization can be used as a guide for introducing relativistic kinematics into nr expressions that are more accurate than the impulse approximation (IA). The advantage here is that applications of such expressions are easier to extend to the calculation of DDCS for larger systems than their fully relativistic versions.

The impulse approximation is the most widely used approach for the prediction of Compton differential cross sections. Some examples of applications of this theory to the prediction of Compton DDCS of light atoms in nonrelativistic (nr) regimes are found in Refs. [1–3]. The nonrelativistic theory, which is what the IA approach was originally based on, starts with a two-term interaction Hamiltonian $H_{\rm int} = (e^2A^2/2m^2) - e(\vec{p}\cdot\vec{A})/m$. This nonrelativistic matrix element corresponds to the A^2 term in $H_{\rm int}$ taken in nonrelativistic first-order QED perturbation theory. This A^2 matrix element largely describes the Compton peak region of the DDCS spectrum. The matrix element resulting from the $\vec{p}\cdot\vec{A}$ term is obtained in second-order QED perturbation theory. This second-order matrix element involves transitions to intermediate states. The infrared rise results as the scattered photon energy decreases, approaching zero. This matrix element also contributes to the Compton peak region, the extent being dependent on photon energies, scattering angle, and Z. Nonrelativistic IA (NRIA) expressions can be derived from the A^2 matrix element. This is based on the assumption that the momentum and energy transfer from an incident photon to a target electron is sufficiently large that the electron binding effects can be neglected, and the bound electrons of the atom are treated as a momentum distribution of free electrons. As a result, one can approximate the final state of the excited electron by a plane-wave state. A purely NRIA result can be derived from the A^2 matrix element, in this way treating the final state as a plane wave and the initial electron as free [4–6]; however, Eisenberger and Platzman [7] showed that this is not necessary for the derivation of the IA result for DDCS.

More than three decades ago it was shown that it is possible to obtain reasonably accurate DDCS in relativistic regimes by using the A^2 matrix element with relativistic kinematics. For example, Schumacher *et al.* [4] used the A^2 matrix element but with a relativistic momentum p_f and energy E_f of the ejected electron to obtain Compton peaks at $\omega_1 = 279$ keV for K-, L-, and M-shell ionization of Cu and Pb. More recently, Costescu and Spanulescu [8] used a more general approach by first

taking the nr limit of the second-order perturbation relativistic QED S-matrix element to obtain expressions for DDCS and triply differential cross sections (TDCS), free of spurious singularities but having a separable A^2 and $\vec{p}\cdot\vec{A}$ form (not separable in the fully relativistic S-matrix expression). He then introduced relativistic kinematics, resulting in expressions that can be used to obtain reasonably accurate K-shell DDCS at all θ if $\omega_1 < 300$ keV. At higher energies this expression only works at smaller scattering angles. This was illustrated by their example calculation in which $\omega_1 = 661$ keV and $\theta \leqslant 60^\circ$.

In NRIA theory, DDCS are proportional to the Compton profile, given by

$$J\left(p_z^{\rm nr},\rho_{\rm nr}\right) = 2\pi \int_{p_z^{\rm nr}}^{\infty} dp\; p\rho_{\rm nr}(p), \tag{1}$$

where p is the initial electron momentum. $\rho_{\rm nr}(p)$ is the Fourier transform of the nr charge density $\rho_{\rm nr}(r)$ for an electron in a given nonrelativistic quantum state. $p_z^{\rm nr}$ is the z component of the initial electron momentum given from conservation of energy and momentum as

$$p_z^{\rm nr} = \left|\frac{(\omega_1-\omega_2)m}{q} - \frac{q}{2}\right|, \tag{2}$$

where ω_1 and ω_2 correspond to the energies of the incident and scattered photons and $q = |\vec{K}_1 - \vec{K}_2|$ is the magnitude of the momentum transfer, where $\vec{K}_1$ and $\vec{K}_2$ represent the momenta of the incident and scattered photons. Also the units $c = \hbar = 1$ apply throughout. The expression for Compton scattering DDCS in terms of the Compton profile $J(p_z^{\rm nr},\rho_{\rm nr})$ [7] is

$$\frac{d^2\sigma}{d\omega_2 d\Omega_2} = K^{\rm nr} J\left(p_z^{\rm nr},\rho_{\rm nr}\right), \tag{3}$$

where Ω_2 is the solid angle for the scattered photon and the nr kinematic factor $K^{\rm nr}$ is given by

$$K^{\rm nr} = \frac{r_0^2 m\omega_2 X^{\rm nr}}{2\omega_1 q}, \tag{4}$$

with $X^{\rm nr} = 1+\cos^2\theta$, where θ is the photon scattering angle and r_0 the classical electron radius.

For relativistic regimes, a widely used version of IA theory was obtained by Ribberfors [9]. In this approach the RIA formula for DDCS is given by Eq. (15) in [9]. Ribberfors derived an explicit expression for DDCS from RIA theory, starting with the relativistic S-matrix formulation of Jauch and Rohrlich for the Compton matrix element [10], namely,

$$\begin{aligned}\frac{d^2\sigma}{d\omega_2 d\Omega_2} &= \frac{m^2 r_0^2\omega_2}{2q\omega_1}\int_{p_{\rm min}}^{\infty}\frac{p\rho_{\rm rel}(p)}{E(p)}\int_0^{2\pi}\bar{X}(p,\zeta)dpd\zeta \\ &= \frac{\pi m^2 r_0^2\omega_2}{q\omega_1}\int_{p_{\rm min}}^{\infty}\frac{p\rho_{\rm rel}(p)\bar{X}_{\rm int}(p)}{E(p)}dp,\end{aligned} \tag{5}$$

where $E(p) = (p^2+m^2)^{1/2}$ is the energy of the initial electron and $\bar{X}(p,\zeta)$ is the relativistic kinematic component [9], a function of ω_1, ω_2, and θ as well as p and ζ, where ζ is the azimuthal angle of the initial electron. $\bar{X}(p,\zeta)$ and its integrated form $\bar{X}_{\rm int}(p) = (1/2\pi)\int_0^{2\pi}\bar{X}(p,\zeta)d\zeta$ will be discussed in Sec. II B. Later Ribberfors [9] obtained a simpler but approximate expression from Eq. (5) by integration by parts over p, then employing the fact that $J(\infty) = 0$ and that the energy of the initial electron $E(p)$ is approximately equal to m, he obtained a more approximate nonrelativistic-form expression, which like the NRIA expression has a separable kinematic factor and Compton profile, to be referred to as the KJ approximation and may be written as

$$\frac{d^2\sigma}{d\omega_2 d\Omega_2} = K^{\rm rel}(p_{\rm min})J(p_{\rm min},\rho_{\rm rel}), \tag{6}$$

where $J(p_{\rm min},\rho_{\rm rel})$ is the relativistic Compton profile, a function of the relativistic charge density $\rho_{\rm rel}$, and the relativistic variable $p_{\rm min}$ [9] used in place of p_z is given by

$$p_{\rm min} = (1/q)|E(p_{\rm min})(\omega_1-\omega_2) - \omega_1\omega_2(1-\cos\theta)|. \tag{7}$$

The relativistic kinematic factor in Eq. (6) is given by

$$K^{\rm rel}(p_{\rm min}) = \frac{r_0^2 m^2\omega_2\bar{X}(p_{\rm min})}{2\omega_1 q E(p_{\rm min})}. \tag{8}$$

$\bar{X}(p_{\rm min})$, the integrated (over p and ζ) form of $\bar{X}(p,\zeta)$ is a function of ω_1, ω_2, and θ, given by Eq. (49) in [9] (also discussed in Sec. II). Equation (6) can be used in place of the full RIA expression [Eq. (5)] provided that the average initial momentum of the ejected electron is small: $\langle p_i\rangle < m$ even if $\omega_1 > m$, for example in the case of K-shell ionization when $Z < 30$. At higher Z this expression yields an overestimation of the magnitude of the Compton peak, but it does give a reasonably accurate prediction for its position on the ω_2 scale. This approximate RIA expression allows one to understand the relativistic contributions to the position and magnitude of the Compton peak in terms of a factorable $K^{\rm rel}(p_{\rm min})$ and $J(p_{\rm min},\rho_{\rm rel})$ and the variables $p_{\rm min}$ and $\rho_{\rm rel}$. A systematic account and analysis for when and why the KJ approximation breaks down will be the subject of a future publication.

Much of the results in this work on inelastic photon atom Compton scattering can also apply to inelastic electron atom collisions in which the atom is ionized, including the $(e,2e)$ experiment. This is because the RIA expression for DDCS for this process has the same form as Eq. (5) for the full RIA expression. Also the inelastic electron scattering expression can as an approximation be placed in the same form as Eq. (6) [11]. Here K and $p_{\rm min}$ are in terms of an initial and scattered electron rather than a photon. Some examples in which such RIA inelastic electron scattering expressions are applicable can be found in [12]. Also, with regard to the $q\to 0$ nr limit, it is a known fact that relativistic effects decrease with decreasing q. For example, when q is sufficiently low, nonrelativistic approximations have been used for calculations of electron scattering off ^{3}He at kinetic energies in the hundreds of MeV [13].

In Sec. II, mathematical and physical arguments are given for how NRIA expressions for DDCS can be recovered from the corresponding RIA expressions in the limit of low momentum transfer ($q\to 0$) provided that $\langle p_i\rangle < m$. This $q\to 0$ nr limit is advantageous, because it is in terms of ω_2 and θ, the differential variables for DDCS, and this limit is valid even at high ω_1 ($\omega_1 > m$). Also it is argued that much of the relativistic kinematic contribution to the Compton peak is associated with the difference between two simple terms, $\omega_1\omega_2$, which is a term in the relativistic $p_{\rm min}$, and $[\omega_1^2+\omega_2^2]/2$, a term in the nr $p_z^{\rm nr}$. This approach allows for an explanation for why one can use nonrelativistic expressions

to obtain accurate predictions for DDCS around the Compton peak when θ is small, even in the 1-MeV range. In Sec. III, examples are given of comparisons between the predictions of DDCS from S-matrix theory [10] and RIA theory [9], for the latter using Eqs. (5) and (6) along with various nonrelativistic modifications of these two equations. Here a discussion is given on the relativistic contributions to the Compton peak due to K and J and their dependence on $p_{\min}$ and $\rho_{\rm rel}$ and the dependence of these two parameters on ω_1, θ, and Z. The results provide a guide for predicting under what circumstances nr expressions can be used to obtain an accurate Compton peak when ω_1 is in the relativistic regime. Finally, characterization of relativistic contributions to Compton DDCS will be discussed for theories that go beyond IA theory in Sec. IV. In this case the example discussed is an improved approach for introducing relativistic kinematics into the A^2 matrix element expression such that it can be used to obtain an accurate Compton peak.

II. KINEMATIC NONRELATIVISTIC LIMIT OF RIA EXPRESSIONS FOR DDCS

The kinematic nonrelativistic limit of both the full [Eq. (5)] and more approximate factorized [Eq. (6)] RIA expressions are obtained in the limit $q \to 0$ by first assuming that the average initial momentum of the ejected electron is such that $\langle p_i \rangle < m$. Then the two nr limits $p_{\min} \to p_z^{\rm nr}$ as $\omega_2 \to \omega_1$ and $\bar{X} \to 1 + \cos^2\theta \to 2$ as $\theta \to 0^\circ$ are taken. The three limits $q \to 0$, $\omega_2 \to \omega_1$, and $\theta \to 0^\circ$ are simultaneous at the Compton profile maximum. In this section the nr limits of $p_{\min}$ and $\bar{X}$ are discussed in Secs. II A and II B, respectively. In Sec. II C, it is shown that the $q \to 0$ nr limit is fundamental in that it also applies to the simplest example of Compton scattering, which is the scattering of a photon off of a stationary free electron. Some of the equations in this section will be used to make the A^2 matrix element expression for DDCS kinematically relativistic.

A. Nonrelativistic limit of $p_{\min}$

The expression for $p_z^{\rm nr}$ can be placed in a form similar to that of $p_{\min}$ by substitution of the explicit formula for the magnitude of momentum transfer, $q = [\omega_1^2 + \omega_2^2 - 2\omega_1\omega_2\cos\theta]^{1/2}$ into Eq. (2). This yields

$$p_z^{\rm nr} = (1/q)\left|m(\omega_1 - \omega_2) + \omega_1\omega_2\cos(\theta) - \left(\omega_1^2 + \omega_2^2\right)/2\right|. \tag{9}$$

It can be argued that if $\langle p_i \rangle < m$ such that the Compton profile and therefore the Compton peak is sufficiently narrow, causing the relevant range of $p_{\min}$ to be much less than m, the result is $E(p_{\min}) = (p_{\min}^2 + m^2)^{1/2} \approx m$. By making these assumptions, Eq. (7) for $p_{\min}$ can be expressed as

$$p_{\min} \approx p_z^{\rm rel} = (1/q)|m(\omega_1 - \omega_2) + \omega_1\omega_2\cos(\theta) - \omega_1\omega_2|. \tag{10}$$

Clearly as the ω_2 at which the Compton peak has its maximum amplitude $\omega_2^{\rm pk}$ approaches ω_1 ($\omega_2^{\rm pk} \to \omega_1$ is simultaneous with $q \to 0$ and $\theta \to 0^\circ$), $p_{\min} \to p_z^{\rm nr}$. In Sec. III, it is shown from numerical calculations that most of the kinematic relativistic contribution to the Compton peak is associated with the difference between $p_{\min}$ and $p_z^{\rm nr}$. This means that such relativistic contributions can be characterized as the difference between the third terms in Eqs. (9) and (10) since the first two terms are identical. Not only does $p_{\min} \to p_z^{\rm nr}$ result when $q \to 0$, it also does when $\omega \ll m$ because ω_1 and ω_2 are small.

Simple expressions for the position of the Compton profile maximum on the ω_2 scale can be obtained from Eq. (10) in the relativistic case by setting $p_{\min} = 0$ and solving for $\omega_2(p_{\min} = 0)$:

$$\omega_2(p_{\min} = 0) = \frac{m\omega_1}{m + \omega_1(1 - \cos\theta)}, \tag{11}$$

and from Eq. (9) by setting $p_z^{\rm nr} = 0$ in the nr case:

$$\omega_2\left(p_z^{\rm nr} = 0\right) = -(m - \omega_1\cos\theta) \pm [(m - \omega_1\cos\theta)^2 - \omega_1(\omega_1 - 2m)]^{1/2}. \tag{12}$$

Both $\omega_2(p_{\min} = 0)$ and $\omega_2(p_z^{\rm nr} = 0)$ at a given ω_1 are smallest when $\theta = 180^\circ$. As θ decreases, both approach ω_1, becoming equal to ω_1 when $\theta = 0$. However, due to conservation of energy, $\omega_1 - \omega_2 = E_k + |E_b|$ (where E_k is the kinetic energy of the ejected electron and E_b is the binding energy of the ejected electron), and $\omega_2(p_{\min} = 0)$ and $\omega_2(p_z^{\rm nr} = 0)$ can never equal ω_1 if the outgoing electron was initially bound. As a result, θ cannot go all the way to zero and still have a Compton peak maximum in the DDCS spectrum without violating conservation of energy. This means that when E_k is zero at the Compton peak maximum, $\theta > 0$ and $\omega_2(p_{\min} = 0)$ and $\omega_2(p_z^{\rm nr} = 0)$ are both less than ω_1 and the nr limit is never quite reached. The smaller $\langle p_i \rangle$ (or E_b) is, the closer is the approach of $p_{\min}$ to its nr limit $p_z^{\rm nr}$. Therefore the true nr limit for the RIA expression for DDCS at the Compton peak results when $\theta \to 0$, not when $E_k \to 0$. In Sec. III C, Eqs. (11) and (12) will be used to calculate the relativistic shift with respect to ω_2 of the position of the Compton profile in the DDCS spectrum such that it can be compared to the relativistic shift of the position of the Compton peak over all θ at various ω_1 and Z.

B. Nonrelativistic limit of the kinematic factor $\bar{X}$

The nr limit of Eq. (5) or (6) is not complete without also taking the nr limit of $\bar{X}$. In Eq. (5) this involves taking the nr limit of $\bar{X}(p,\zeta)$ and $E(p)$ and in Eq. (6) the nr limits of $\bar{X}(p_{\min})$ and $E(p_{\min})$. Both $\bar{X}(p,\zeta)$ and $\bar{X}(p_{\min})$ are given by expressions of the same form:

$$\bar{X} = \frac{R}{R'} + \frac{R'}{R} + 2m^2\left[\frac{1}{R} - \frac{1}{R'}\right] + m^4\left[\frac{1}{R} - \frac{1}{R'}\right]^2, \tag{13}$$

only differing in the expressions for R and R'. For both Eqs. (5) and (6)

$$R' = R - \omega_1\omega_2(1 - \cos\theta), \tag{14}$$

where R for Eq. (5) is given by

$$R(p,\zeta) = \omega_1[E(p) - D(p) - H(p)\cos\zeta], \tag{15}$$

where $E(p) = [p^2 + m^2]^{1/2}$, D, and H are given by [9]

$$D(p) = (\omega_1 - \omega_2\cos\theta)(p\cos\beta)/q, \tag{16}$$

β is the angle between the vectors for momentum transfer and that of the initial electron, and

$$H(p) = (\omega_2 \sin\theta p \sin\beta)/q = \omega_2 \sin\theta\left(p^2 - p_{\min}^2\right)^{1/2}/q. \tag{17}$$

$R(p_{\min})$ for Eq. (6) is given by

$$R(p_{\min}) = \omega_1[E(p_{\min}) - D(p_{\min})], \tag{18}$$

where $E(p_{\min}) = [p_{\min}^2 + m^2]^{1/2}$, $D(p_{\min})$ is given by [9]

$$D(p_{\min}) = (\omega_1 - \omega_2\cos\theta)p_{\min}/q, \tag{19}$$

and $H(p_{\min}) = 0$.

The nr limit of $E(p)$ in Eq. (5) is valid around the Compton peak maximum since the maximum amplitude of the Compton profile occurs at $p_{\min} = 0$ with $J(\infty, \rho_{\rm rel}) = 0$. The assumption that $p < m$ over the range of p at which $J(p,\rho)$ has a significant value is valid if J is sufficiently narrow (the smaller $\langle p_i\rangle$ becomes, the more narrow J becomes). With these assumptions, $E(p)$ becomes nearly constant and approximately equal to m. In the case of Eq. (6), $E(p_{\min}) \approx m$ around the Compton peak (see Sec. II A). The nr limits of $\bar{X}(p,\zeta)$ in Eq. (5) and $\bar{X}(p_{\min})$ in Eq. (8) [for Eq. (6)] can then be obtained when $\theta \to 0$, resulting in $\omega_1\omega_2(1-\cos\theta) \to 0$ in Eq. (14), making $R \approx R'$, even if ω_1 is high. Then in Eq. (13), $(1/2\pi)\bar{X}(p,\zeta) \to \bar{X}(p_{\min}) \to X^{\rm nr} = 1 + \cos^2\theta \to 2$. As a result, the kinematic factors in Eq. (5), which includes $\bar{X}$, $E(p)$, and the p-independent factor $m^2r_0^2\omega_2/2q\omega_1$ [integration over $\bar{X}(p,\zeta)$ in the $\theta \to 0^\circ$ limit with respect to ζ in Eq. (5) yields $2\pi X^{\rm nr}$, where 2π is part of J as in Eq. (1)] reduce to $K^{\rm nr}$ [Eq. (4)]. Also $K^{\rm rel}$ [Eq. (8)] reduces to $K^{\rm nr}$ [for Eq. (6)]. The results of the $\theta \to 0$ limit, the nr limit for $p_{\min} \to p_z^{\rm nr}$ as $\omega_2^{\rm pk} \to \omega_1$ (where $\omega_2^{\rm pk}$ is the ω_2 at which the Compton peak is at its maximum amplitude), along with the assumption $\langle p_i\rangle < m$, resulting in $\rho_{\rm rel} \to \rho_{\rm nr}$ (see Sec. III B), make it possible for Eq. (3) to be obtained from the low-momentum-transfer nr limits of Eqs. (5) or (6) at the Compton peak.

There is an alternate way to obtain the $q \to 0$ nr limit of Eq. (5). This involves starting with the expression for $\bar{X}_{\rm int}$, which is the integrated (over ζ) form of $\bar{X}$ and is given by [9]

$$\begin{aligned}\bar{X}_{\rm int}(p) = \frac{1}{2\pi}\int_0^{2\pi}\bar{X}d\zeta = 2 + F\left\{\frac{1}{[(E-W-D)^2 - H^2]^{1/2}}\right.\\ \left. - \frac{1}{[(E-D)^2 - H^2]^{1/2}}\right\}\\ + \frac{m^2}{\omega_1^2}\left\{\frac{E-D}{[(E-D)^2 - H^2]^{3/2}}\right.\\ \left. + \frac{E-W-D}{[(E-W-D)^2 - H^2]^{3/2}}\right\},\end{aligned} \tag{20}$$

where

$$F = W - \frac{2m^2}{\omega_1} - \frac{2m^4}{\omega_1^2 W}, \tag{21}$$

$$W = \omega_2(1-\cos\theta). \tag{22}$$

If one assumes that as $\langle p_i\rangle \to 0$, then $p_{\max} \to p_{\min} \to 0$ (where $p_{\max}$ is the highest $|p_{\min}|$ at which the Compton profile has a significant magnitude, located at the tail region J), then $E \to m$, $D \to 0$, and $H \to 0$ and substitution of Eqs. (21) and (22) into (20) yields

$$\begin{aligned}\bar{X}_{\rm int}^{\langle p_i\rangle\to 0} = 2 + \left[\left(W - \frac{2m^2}{\omega_1} + \frac{2m^4}{\omega_1^2 W}\right)\left(\frac{1}{m-W} - \frac{1}{m}\right)\right]\\ + \frac{m^4}{\omega_1^2}\left[\frac{1}{m^2} + \frac{1}{(m-W)^2}\right].\end{aligned} \tag{23}$$

After substitution of

$$\omega_1 = \frac{m\omega_2(p_{\min}=0)}{m - \omega_2(p_{\min}=0)(1-\cos\theta)} \tag{24}$$

[obtained from rearrangement of Eq. (11)] into Eq. (23), the result is

$$\bar{X}_{\rm int}^{\langle p_i\rangle\to 0} = \frac{[\omega_2(1-\cos\theta)]^2}{m[m - \omega_2(1-\cos\theta)]} + 1 + \cos^2\theta. \tag{25}$$

Thus the nonrelativistic limit $\bar{X}_{\rm int}^{\rm nr} = 1 + \cos^2\theta$ results either when $\theta \to 0^\circ$ or when $\omega \ll m$. Both limits require $\langle p_i\rangle < m$ (low E_b or Z). Using this along with the $\omega_2 \to \omega_1$ limit, which yields the limit $p_{\min} \to p_z^{\rm nr}$, and $\rho_{\rm rel} \to \rho_{\rm nr}$ as $\langle p_i\rangle \to 0$, one obtains the nr expression from the RIA expression for DDCS [Eq. (5)]. The $\omega_1 \ll m$ nr limit can also be obtained for the nonintegrated $\bar{X}(p,\zeta)$ in a similar way.

$\bar{X}(p_{\min})$ is greatest when $\theta = 180^\circ$, increasing with increasing ω_1 especially if θ is large (see Fig. 1). As θ decreases to less than about 35°, the three $X(p_{\min})$ curves begin to merge with the $X^{\rm nr} = 1 + \cos^2\theta$ curve. This suggests that one can use $X^{\rm nr}$ to calculate DDCS at the Compton peak when $\theta < 35^\circ$ even at energies as high as 1 MeV. Finally, if one considers $\bar{X}(p_z^{\rm nr})$ (heavy dashed curves) it is clear that it never exceeds 2 at any energy or angle and like $\bar{X}(p_{\min})$ merges with the $X^{\rm nr}$ curve, ultimately going to 2 as θ goes to zero. Interestingly $\bar{X}(p_z^{\rm nr})$ appears to saturate at 2 at all θ as ω_1 becomes increasingly larger. This suggests that much of the non-ρ relativistic contribution to the Compton peak magnitude is due to the difference between $\bar{X}(p_{\min})$ and $\bar{X}(p_z^{\rm nr})$. The relativistic shift is due almost entirely to the difference between $\omega_1\omega_2$ in $p_{\min}$ and $(\omega_1^2 + \omega_2)/2$ in $p_z^{\rm nr}$. Also, as the relativistic

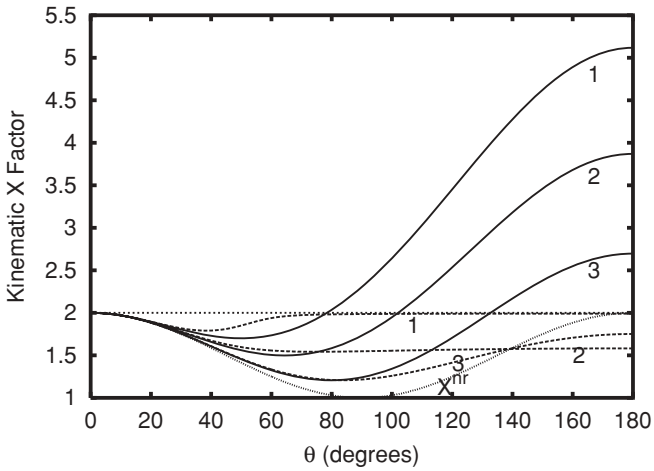

FIG. 1. θ dependence of the kinematic factor X at the Compton peak maximum. $\bar{X}(p_{\min})$ [see Eqs. (13) and (18)], solid lines; $\bar{X}(p_z^{\rm nr})$, short heavy dashed lines; $X^{\rm nr} = 1 + \cos^2\theta$, fine dotted line: 1. 1.00 MeV, 2. 662 keV, and 3. 320 keV.

shift increases, the increase in the peak magnitude is enhanced due to the increase of ${}^{\rm rel}\omega_2^{\rm pk}/{}^{\rm nr}\omega_2^{\rm pk}$, where ${}^{\rm rel}\omega_2^{\rm pk}$ and ${}^{\rm nr}\omega_2^{\rm pk}$ correspond to the $\omega_2^{\rm pk}$ for the RIA [Eq. (5)] and NRIA [Eq. (3)] expressions for DDCS, respectively.

The results in Secs. II A and II B suggest that one can use nonrelativistic kinematics for small-angle scattering around the Compton peak even at relativistic photon energies. One can use Eqs. (11) and (12) to predict when one can use nr expressions for the calculation of the Compton peak even at high ω_1 if E_b for the ejected electron is less than around 20 keV. At higher E_b these formulas can still give a rough estimate for when nr expressions apply; however, as E_b approaches 100 keV, the kinematic factors can substantially alter the shape and $\omega_2^{\rm pk}$ of the Compton peak. A systematic analysis of the ranges of ω_1, θ, and Z under which the $q \to 0$ nr limit is valid will be given in Sec. III C.

C. The low-momentum-transfer nr limit of the kinematic expression for inelastic photon scattering off a free stationary electron

Here it is shown that the $q \to 0$ nr limit is valid for the kinematic expression for the simplest case of Compton scattering, which is inelastic scattering of a photon off a free stationary electron. Some of the formulas in the following will be used to make the A^2 matrix element kinematically relativistic (see Sec. IV). Here the magnitude of the momentum of the electron after photon scattering, p_f, is equal to the photon momentum transfer to the electron (due to conservation of momentum), that is,

$$p_f = q = \left[\omega_1^2 + \omega_2^2 - 2\omega_1\omega_2\cos\theta\right]^{1/2}. \tag{26}$$

The nonrelativistic momentum of the ejected electron is given by

$$p_f^{\rm nr} = [2mE_k]^{1/2}, \tag{27}$$

where E_k is the kinetic energy of the ejected electron. The relativistic momentum is given by

$$p_f^{\rm rel} = \left[E_k^2 + 2mE_k\right]^{1/2}. \tag{28}$$

Also the nonrelativistic energy of the ejected electron is given by

$$E_f^{\rm nr} = m \tag{29}$$

and the relativistic energy by

$$E_f^{\rm rel} = m + E_k. \tag{30}$$

The spectrum of photon scattering off a free stationary electron consists of a narrow band that occurs at a discrete ω_2 rather than a peak over a range of ω_2 as in atomic scattering. Therefore the limits $\theta \to 0$, $\omega_2 \to \omega_1$, and $q \to 0$ are always simultaneous. In the low-ω nr limit, as $\omega \to 0$, q also approaches zero. Then in Eq. (26) as $q \to 0$, $p_f \to 0$ and $E_k \to 0$. This results in $p_f^{\rm rel} \to p_f^{\rm nr}$ and $E_f^{\rm rel} \to E_f^{\rm nr}$. Clearly, both the $q \to 0$ and $\omega \ll m$ limits in this case are essentially the same.

One can understand the relativistic shift of the Compton peak in scattering of a photon off a bound electron in terms of this simple free-electron experiment. From Eqs. (26)–(28), for a given ω_1 and θ it is clear that the condition $p_f^{\rm rel} = q$ requires a higher ω_2 ($\omega_2^{\rm pk}$) than when $p_f^{\rm nr} = q$, because $p_f^{\rm rel} \geqslant p_f^{\rm nr}$. The relativistic shift will increase with increasing ω_1 at a fixed θ. It also increases with increasing θ at a fixed ω_1.

III. CHARACTERIZATION OF THE RELATIVISTIC CONTRIBUTIONS TO COMPTON DDCS

In this section, the relativistic contributions to the Compton peak magnitude and position are characterized using the full (5) and the more approximate factorized (6) RIA expressions. In Sec. III A, using Eq. (6) the various relativistic components that affect the Compton peak magnitude and position are investigated. Equation (6), although it is approximate, allows one to assess the relativistic contribution to the peak magnitude due to the dependence of the kinematic factor $K(p_{\rm min})$ on $p_{\rm min}$ as well as the dependence of $J(p_{\rm min},\rho_{\rm rel})$ on $\rho_{\rm rel}$ and to assess the relativistic contribution to the peak position due to the dependence of $J(p_{\rm min},\rho_{\rm rel})$ on $p_{\rm min}$. Equation (5) could be used here; however, determining the separate contributions of K and J would not be possible. Also Eq. (6) only loses its accuracy when E_b is greater than about 10 keV and the inaccuracy is only reflected in the Compton peak magnitude, not its position. Doubly differential cross sections were obtained from relativistic second-order perturbation S-matrix expressions [10] using the code of Bergstrom and co-workers [14] with a Dirac Slater potential. Doubly differential cross sections from S-matrix calculations are used as a standard for assessing the accuracy of results obtained from RIA [9] and NRIA [6,7] expressions. All calculated Compton DDCS are done within the independent particle approximation and are therefore inclusive. In Sec. III B the Z dependence of the relativistic contribution to the Compton peak magnitude due to K-shell $\rho_{\rm rel}$ is investigated by comparing $J(p_{\rm min},\rho_{\rm rel})$ to $J(p_{\rm min},\rho_{\rm nr})$ at various Z. Also the nr limit $\rho_{\rm rel} \to \rho_{\rm nr}$, which is nonkinematic in that it remains relativistic as $q \to 0$ (as well as when $\omega \ll m$), is discussed. In Sec. III C Eqs. (3) and (5) are used to obtain the relativistic shifts and increases in the Compton peak magnitude over all θ at chosen ω_1 and Z. The purpose is to provide the necessary information that one can use to determine when one can use nr expressions to obtain an accurate Compton peak at high ω_1.

All DDCS from IA expressions were obtained from hydrogenlike wave functions. This is a good approximation because screening effects are negligible for the K-shell ionization of moderate to heavy atoms. Doubly differential cross sections from NRIA theory using Eq. (3) were obtained by using the following expression:

$$J(p_z,\rho_{\rm nr}) = \int_{p_z}^{\infty} p\rho_{\rm nr}(p)dp = \frac{(2\alpha Zm)^5}{12\pi\left[p_z^2 + (\alpha Zm)^2\right]^3}. \tag{31}$$

Doubly differential cross sections obtained by using Eq. (6) in which $\rho_{\rm rel}$ is replaced by $\rho_{\rm nr}(p) = \chi^2(p)$ are obtained from the Fourier transform of the nr radial hydrogenlike wave function given by

$$\chi(p) = \frac{2^{3/2}(\alpha Zm)^{5/2}}{\pi^{1/2}[(\alpha Zm)^2 + p^2]^2}. \tag{32}$$

In the relativistic case where $\rho_{\rm rel}(p) = [G^2(p) + F^2(p)]$ the expression

$$J(p_{\rm min}, \rho_{\rm rel}) = \int_{p_{\rm min}}^{\infty} p[G^2(p) + F^2(p)]dp, \qquad (33)$$

which involves numerical integration over p, is used. $G(p)$ and $F(p)$ are the Fourier transforms of the corresponding radial Dirac large $G(r)$ and small $F(r)$ component hydrogenlike wave functions, given by the following expressions:

$$G(p) = (2\alpha Zm)^{\gamma+1/2} C^+ \frac{\gamma \sin\left[(\gamma+1)\tan^{-1}\left(\frac{p}{\alpha Zm}\right)\right]}{\pi^{1/2} p[p^2 + (\alpha Zm)^2]^{\frac{(\gamma+1)}{2}}}, \qquad (34)$$

$$F(p) = \frac{(2\alpha Zm)^{\gamma+1/2} C^- \left\{ \frac{\sin[\gamma \tan^{-1}(\frac{p}{\alpha Zm})]}{p} - \frac{\gamma \cos[(\gamma+1)\tan^{-1}(\frac{p}{\alpha Zm})]}{[p^2+(\alpha Zm)^2]^{1)/2}} \right\}}{\pi^{1/2} p[p^2 + (\alpha Zm)^2]^{\frac{\gamma}{2}}} \qquad (35)$$

where

$$C^{\pm} = \left\{ \frac{1 \pm \left[1 + \left(\frac{\alpha Z}{\gamma}\right)^2\right]^{-1/2}}{2\Gamma(2\gamma+1)} \right\}^{1/2}, \qquad (36)$$

with $\gamma = [1 - (\alpha Z)^2]^{1/2}$. These expressions are used for calculating DDCS from Eq. (5) as well as $J(p_{\rm min}, \rho_{\rm rel})$ in Eq. (6).

A. Identification of the relativistic contributions to the Compton peak

Doubly differential cross section predictions obtained from RIA expressions and nonrelativistic modifications of it, along with S-matrix theory, for Cu ($Z = 29$) with $\omega_1 = 662$ keV and $\theta = 180^\circ$, are given in Fig. 2. See Refs. [15–18] for some examples of the many measurements and calculations done on Compton DDCS at high ω_1. A value of $\theta = 180^\circ$ was chosen to maximize relativistic effects on the Compton peak magnitude. The Compton peak predictions from S-matrix (designated by peak 1 in Fig. 3) and RIA expressions using Eq. (5) (peak 2) yield a maximum peak amplitude located at $\omega_2^{\rm pk} = 188$ keV, which corresponds to an ejected electron velocity of v_e/c of 0.84. The predicted DDCS obtained from Eq. (6), designated by peak 3, although an approximation of Eq. (5), is in good agreement with peaks 1 and 2. From these results one can conclude that the full RIA expression of Ribberfors [Eq. (5)] as well as his approximation [Eq. (6)] of Eq. [5] works well, for a light element at $\omega_1 = 662$ keV.

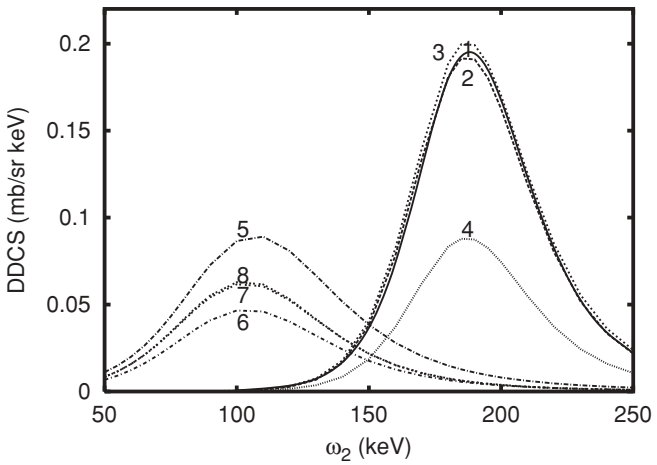

FIG. 2. Doubly differential cross sections for copper ($Z = 29$), K-shell ionization, $\omega_1 = 662$ keV. and $\theta = 180^\circ$. Curves are labeled as follows: 1, S-matrix, solid line; 2, RIA based on Eq. (5), short heavy dashes; 3, RIA based on Eq. (6), heavy dots; 4, Eq. (6) with $K^{\rm rel}(p_z^{\rm nr})$, $J(p_{\rm min}, \rho_{\rm rel})$, fine dots; 5, Eq. (6) with $K^{\rm rel}(p_{\rm min})$, $J(p_z^{\rm nr}, \rho_{\rm rel})$, dots and long dashes; 6, Eq. (6) with $K^{\rm rel}(p_z^{\rm nr})$, $J(p_z^{\rm nr}, \rho_{\rm rel})$, dots and short dashes; 7, Eq. (6) with $K^{\rm nr}$, $J(p_z^{\rm nr}, \rho_{\rm rel})$, dots in pairs; 8, Eq. (6) with $K^{\rm nr}$, $J(p_z^{\rm nr}, \rho_{\rm nr})$ fully nonrelativistic [NRIA, same as Eq. (3)], dots in triples.

The effects of replacing $p_{\rm min}$ by $p_z^{\rm nr}$ in K of Eq. (6) are shown [i.e., $K^{\rm rel}(p_{\rm min})$, $J(p_{\rm min}, \rho_{\rm rel}) \rightarrow K^{\rm rel}(p_z^{\rm nr})$, $J(p_{\rm min}, \rho_{\rm rel})$ for peak $3 \rightarrow 4$]. The magnitude of the resulting Compton peak 4 is reduced by more than 60% and its position is only slightly altered (compared to peak 3). If $p_{\rm min}$ is replaced by $p_z^{\rm nr}$ in J but not K [i.e., $K^{\rm rel}(p_{\rm min})$, $J(p_{\rm min}, \rho_{\rm rel}) \rightarrow K^{\rm rel}(p_{\rm min})$, $J(p_z^{\rm nr}, \rho_{\rm rel})$ for peak $3 \rightarrow 5$] the result is a peak shift to lower ω_2 by about 82 keV with about a 50% reduction of the peak magnitude, which is largely due to $\omega_2^{\rm pk}$ being smaller for peak 5 compared to 3 and the DDCS magnitude being proportional to ω_2 [see Eq. (8)], but with a substantial contribution due to the difference between $\bar{X}(p_{\rm min})$ at $\omega_2^{\rm pk} = 188$ keV and at $\omega_2^{\rm pk} = 106$ keV and a smaller contribution due to q, which is also a function of ω_2. If K and J are both functions of $p_z^{\rm nr}$ [i.e., $K^{\rm rel}(p_{\rm min})$, $J(p_{\rm min}, \rho_{\rm rel}) \rightarrow K^{\rm rel}(p_z^{\rm nr})$, $J(p_z^{\rm nr}, \rho_{\rm rel})$ for peak $3 \rightarrow 6$], the resulting peak 6 has a magnitude more than 75% less than peak 3 and is located at $\omega_2^{\rm pk} = 106$ keV, which is about 82 keV lower than the $\omega_2^{\rm pk}$ of peak 3. Next the kinematic factor is made completely nonrelativistic in Eq. (6); by replacing $K^{\rm rel}(p_z^{\rm nr})$ [Eq. (8)] by $K^{\rm nr}$ [Eq. (4)], the resulting peak, 7, has a somewhat greater magnitude than 6 [i.e., $K^{\rm rel}(p_z^{\rm nr})$, $J(p_z^{\rm nr}, \rho_{\rm rel}) \rightarrow K^{\rm nr}$, $J(p_z^{\rm nr}, \rho_{\rm rel})$ for peak $6 \rightarrow 7$]. Finally, Eq. (6) becomes completely nonrelativistic [NRIA, equivalent to Eq. (3)] when $\rho_{\rm rel}$ replaces $\rho_{\rm nr}$; the resulting peak, 8 [i.e., $K^{\rm nr}$, $J(p_z^{\rm nr}, \rho_{\rm rel}) \rightarrow K^{\rm nr}$, $J(p_z^{\rm nr}, \rho_{\rm nr})$ or peak $7 \rightarrow 8$], is very similar to peak 7, demonstrating a nearly negligible relativistic effect due to $\rho_{\rm rel}$ on DDCS. These comparisons show that most of the relativistic effect on the Compton peak within RIA theory is associated with the difference between $p_{\rm min}$ and $p_z^{\rm nr}$, confirming conclusions based on the result given in Fig. 1.

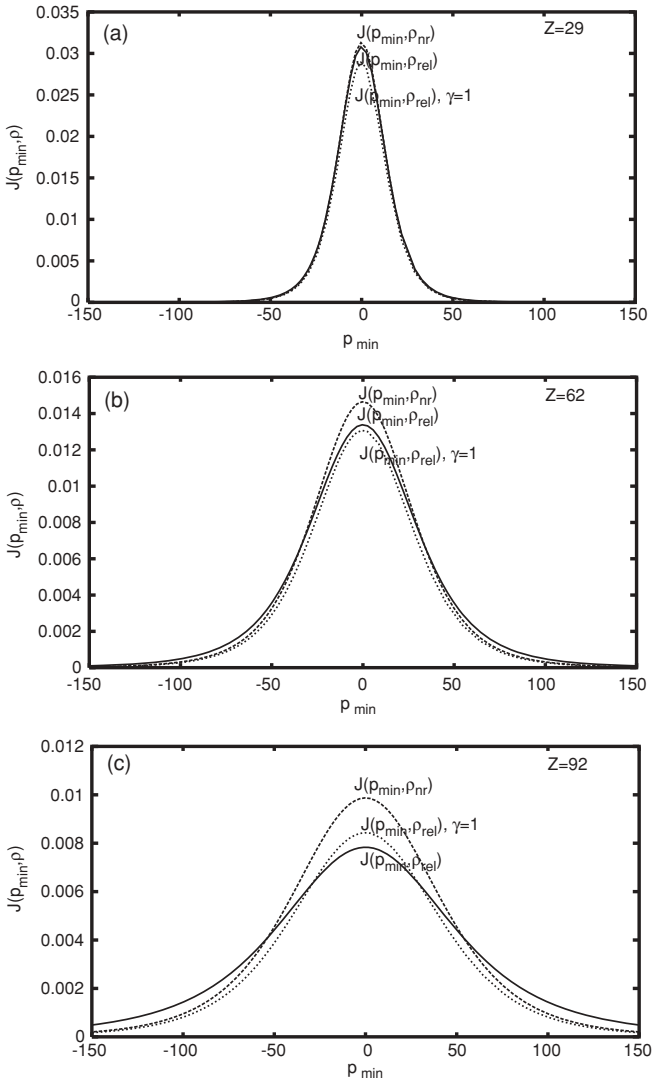

FIG. 3. Z dependence of the K-shell Compton profile as a function of $p_{\min}$: $J(p_{\min},\rho_{\rm rel})$, solid line; $J(p_{\min},\rho_{\rm nr})$; short heavy dashed line; and $J(p_{\min},\rho_{\rm rel})$ with $\gamma=1$, heavy dots. The units are defined as $\hbar=c=1$. (a) $Z=29$; (b) $Z=62$; (c) $Z=92$.

B. Relativistic contribution of the K-shell $\rho_{\rm rel}$ to the Compton profile

Here a discussion is given on how relativistic effects due to $\rho_{\rm rel}$ affect the magnitude and shape of the Compton profile. See, for example, [19,20] for measurements and calculations of the Compton profiles of heavy atoms. The position of the Compton profile J on the ω_2 scale is determined by where $p_{\min}$ [Eq. (11)] or in the nr case by where $p_z^{\rm nr}$ [Eq. (12)] is zero. As $q\to 0$ the Compton profile moves to higher ω_2 and its position is dependent on ω_1 and θ. However, the magnitude and shape of J are not changed unless Z is changed. If Z is changed the position of J is not altered; however, the shape and magnitude of the Compton peak are indirectly affected with changing Z due to the presence of kinematic factors (see Sec. III C). In IA theory, not only does the Compton profile always have its maximum amplitude at $p_{\min}=0$ or $p_z^{\rm nr}=0$, it is always symmetrical with respect to the zero position.

The results in Fig. 3 are obtained from Eqs. (31) and (33). In Eq. (31) $p_z^{\rm nr}$ is replaced by $p_{\min}$. The nr limit of $G(p)$ is $\chi(p)$ and that of $F(p)$ is zero [see Eqs. (32) and (34)–(36)]. Here this nr limit is due to two limits: $\gamma\to 1$ and $p\to 0$, both simultaneous with $Z\to 0$. The $p\to 0$ limit results as the Compton profile narrows with decreasing Z ($\langle p_i\rangle$) (see arguments in Sec. II B). The nr limits of $G(r)$ and $F(r)$ involve $\gamma\to 1$ but not $p\to 0$. In Fig. 3 a comparison is made among $J(p_{\max},\rho_{\rm rel})$, $J(p_{\max},\rho_{\rm rel})$ with $\gamma=1$, and $J(p_{\max},\rho_{\rm nr})$. This shows the total relativistic contribution to J due to the $\gamma\to 1$ [compare $J(p_{\min},\rho_{\rm rel})$ to $J(p_{\min},\rho_{\rm rel})$ with $\gamma=1$], where $F(p)\to 0$, and that due to $p\to 0$ [compare $J(p_{\min},\rho_{\rm rel})$ with $\gamma=1$ to $J(p_{\min},\rho_{\rm nr})$]. Here $f_{\max}$ is defined as the percentage of the contribution of the small component wave function, $F(p)$ [Eq. (35)], to the Compton profile amplitude at its maximum. When $Z=29$ [$\gamma=0.98$, $f_{\max}=1.6\%$], the difference in the maximum amplitude between $J(p_{\min},\rho_{\rm rel})$ and $J(p_{\min},\rho_{\rm nr})$ is nearly negligible, with the magnitude of the latter less than 2% greater than the former at $p_{\min}=0$. This confirms that one can use $\rho_{\rm nr}$ to calculate DDCS at any energy and θ if $Z<30$. However, as Z increases above 29 the differences between $J(p_{\min},\rho_{\rm rel})$ and $J(p_{\min},\rho_{\rm nr})$ increase. This difference in the magnitude between $J(p_{\min},\rho_{\rm rel})$ and $J(p_{\min},\rho_{\rm nr})$ is about 9.5% when $Z=62$ ($\gamma=0.89$, $f_{\max}=7.3\%$) and is about 26% when $Z=92$ ($\gamma=0.74$, $f_{\max}=16.4\%$), an increase that is proportional to Z^2. The difference in the shape of the relativistic and nonrelativistic Compton profiles becomes more apparent with increasing Z. The curves cross, with the relativistic Compton profile magnitude exceeding the nonrelativistic one at high $|p_{\min}|$. It is clear from Fig. 3 that, with increasing Z, this relativistic effect around the maximum amplitude and at the tails of the Compton profile becomes progressively greater. These effects are partly due to the increase of $f_{\max}$ with increasing Z. Most of the rest of the effect on the tails is due to the effect $\gamma\to 1$ has on $G(p)$. The $p\to 0$ factor appears to have its greatest influence around the Compton profile maximum.

The Compton profile at its maximum increases in magnitude and becomes more narrow with decreasing Z. As Z decreases the contribution of the small component $F(p)$ to J rapidly decreases. This is largely because as $\gamma\to 1$, $C^+\to 2^{-1/2}$ while $C^-\to 0$. However, the decrease in the contribution of $F(p)$ to J is enhanced by $p\to 0$ because $G(p)/N^+\to 1/(\alpha Zm)^3$ while $F(p)/N^-\to 0$ [$N^+=(2\alpha Z)^{\gamma+1/2}C^+/\pi^{1/2}$] and [$N^-=(2\alpha Z)^{\gamma+1/2}C^-/\pi^{1/2}$]. Thus as Z becomes small, $F(p)\to 0$, $G(p)\to\chi(p)$, and $\rho_{\rm rel}$ behaves more like $\rho_{\rm nr}$. Then the Compton profile magnitude at $p_{\min}=0$ continues to increases now in proportion to $1/Z$. In this limit J also becomes more narrow because $E_b=\alpha Zm$ decreases and $p_{\min}$ or p_z must also become progressively smaller in order for J to have a significant magnitude.

The relativistic decrease in the Compton peak associated with the dependence of the Compton profile J on $\rho_{\rm rel}$ also applies to the DDCS peak that results from the inelastic electron atom collisions with ionization, since the RIA expression for that process can also be expressed approximately in DDCS = KJ form [11] as in the inelastic photon-atom scattering case. However, the dependence of J on $p_{\min}$ will be somewhat

different because the inelastic electron scattering version of this parameter is somewhat different.

C. ω_1, θ, and Z dependence of the relativistic shift and increase in magnitude of the Compton peak

Here the dependence of the size of the K-shell Compton peak relativistic shift $\Delta\omega_2^{\rm pk}$ and the extent of the relativistic increase in the Compton peak magnitude $R^{\rm rel}$ over all θ are evaluated at selected ω_1 and Z. The effect that ω_1 and Z has on $\Delta\omega_2^{\rm pk}$ and $R^{\rm rel}$ as well as their respective approach to the nr limit is analyzed.

In Fig. 4, the relativistic shift on the scale of ω_1 is defined as $\Delta\omega_2^{\rm rel} = [{}^{\rm rel}\omega_2^{\rm pk} - {}^{\rm nr}\omega_2^{\rm pk}]/\omega_1$, where ${}^{\rm rel}\omega_2^{\rm pk}$ and ${}^{\rm nr}\omega_2^{\rm pk}$ are the positions of the RIA and the corresponding NRIA Compton peak maxima, respectively. These relativistic shifts are compared to the shifts of the Compton profile where $\Delta\omega_2^{\rm rel} = [\omega_2(p_{\rm min}=0) - \omega_2(p_z^{\rm nr}=0)]/\omega_1$ [where $\omega_2(p_{\rm min}=0)$ and $\omega_2(p_z^{\rm nr}=0)$ are defined by Eqs. (11) and (12), respectively]. In Table I the minimum that θ can be and still have a Compton peak maximum in the DDCS spectrum is represented by $\theta_{\rm min}$. Values of $\theta_{\rm min}$ for various ω_1 and Z are given. The maximum θ at which one is within an $n\%$ level of convergence is also given for these variables. For example, when $\omega_1 = 1.0$ MeV and $Z = 15$, $\Delta\omega_2^{\rm rel}$ is within 0.1% of convergence (on the scale of ω_1) when $2.8^\circ \leqslant \theta \leqslant 10.6^\circ$. In this case, a 0.1% level of convergence corresponds to a relativistic shift of 1 keV and the RIA and NRIA Compton peaks are virtually indistinguishable on the DDCS spectrum. Finally, in Table I, $\theta_{\rm max}$ is defined as the θ at which $\Delta\omega_2^{\rm rel}$ is at a maximum.

The approach of $\Delta\omega_2^{\rm rel}$ to zero as $\theta \to 0^\circ$, which is actually due to the simultaneous limit $\omega_2^{\rm pk} \to \omega_1$ improving with decreasing Z, since $\theta_{\rm min}$ decreases due to conservation of energy. The convergence of $\Delta\omega_2^{\rm rel}$ is well within 1% of ω_1 in the DDCS spectrum at all ω_1 when $Z < 62$. Not surprisingly $\Delta\omega_2^{\rm rel}$ increases with increasing ω_1, while the $\theta_{\rm max}$ decreases, eventually approaching 0°, as ω_1 continues to increase into the MeV range. This approach of $\theta_{\rm max}$ to zero can be explained in the context of the Compton profile, labeled CPF in Fig. 4. The reason for this behavior is that the approach of $\omega_2(p_z^{\rm nr}=0)$ [see Eq. (12)] to ω_1 with decreasing θ lags behind the approach of $\omega_2(p_{\rm min}=0)$ [see Eq. (11)] to ω_1 at intermediate θ due to $\omega_2(p_z^{\rm nr}=0)$ being quadratic and having terms of differing sign and powers of $\cos\theta$. At a given ω_1, $\Delta\omega_2^{\rm rel}$ increases and $\theta_{\rm max}$ decreases with decreasing Z, approaching the limit of $\Delta\omega_2^{\rm rel}$ for the Compton profile (CPF). This Z dependence is due to the effect that the kinematic factors have on the Compton profile. As ω_1 increases, this approach to the Compton profile limit requires a progressively lower Z. When $\omega_1 = 320$ keV and $Z = 92$, $\Delta\omega_2^{\rm rel}$ is higher than the CPF curve because the impulse approximation loses its validity with increasing Z and decreasing ω_1.

Figure 5 shows the θ dependence of the ratio $R^{\rm rel} = A^{\rm rel}/A^{\rm nr}$ of the maximum magnitude of the RIA Compton peak $A^{\rm rel}({\rm at}\ {}^{\rm rel}\omega_2^{\rm pk})$ to that of the NRIA Compton peak magnitude $A^{\rm nr}({\rm at}\ {}^{\rm nr}\omega_2^{\rm pk})$. One sees that $R^{\rm rel}$ is strongly influenced by $\bar{X}$ (see Fig. 1), the ratio ${}^{\rm rel}\omega_2^{\rm pk}/{}^{\rm nr}\omega_2^{\rm pk}$, with a smaller effect due to the dependence of q on ω_2. The size of $R^{\rm rel}$ as well as its approach to unity is dependent on $\rho_{\rm rel}/\rho_{\rm nr}$. $R^{\rm rel}$ is greatest at large θ, especially if Z is low. $R^{\rm rel}$ increases with increasing ω_1. This is partly due to $\bar{X}({}^{\rm rel}\omega_2^{\rm pk})/\bar{X}({}^{\rm nr}\omega_2^{\rm pk})$, but there is a potentially larger scale up due to ${}^{\rm rel}\omega_2^{\rm pk}/{}^{\rm nr}\omega_2^{\rm pk}$, which is especially large when ω_1 is in the MeV range, where ${}^{\rm nr}\omega_2^{\rm pk}$ shifts to a very low ω_2. $R^{\rm rel}$ is somewhat affected by $q({}^{\rm nr}\omega_2^{\rm pk})/q({}^{\rm rel}\omega_2^{\rm pk})$ [see Eqs. (3) and (5)]. $R^{\rm rel}$ for a given ω_1 decreases with increasing Z because $\rho_{\rm rel}/\rho_{\rm nr}$ decreases and because the error caused by treating K and J in Eq. (3) as factorable increases. Like $\Delta\omega_2^{\rm rel}$, the approach of $R^{\rm rel}$ to the nr limit as $\theta \to 0^\circ$ improves with decreasing Z. At $\theta_{\rm min}$, the convergence of $R^{\rm rel}$ is to within 1% when $Z = 15$, 3% for $Z = 29$, then rapidly becomes poorer as Z exceeds 60 (also see Table I).

There are two relativistic factors that do not disappear as $\theta \to 0^\circ$: $\rho_{\rm rel}/\rho_{\rm nr}$ (to be referred to as the ρ factor) and the KJ factor, which results in treating K and J in Eq. (3) [also

TABLE I. ω_1, θ, and Z dependence of the relativistic peak shift $\Delta\omega_2^{\rm pk}$ and increase in its magnitude $R^{\rm rel}$. $\Delta\omega_2^{\rm pk} = \frac{{}^{\rm rel}\omega_2^{\rm pk} - {}^{\rm nr}\omega_2^{\rm pk}}{\omega_1}$ and $R_{\rm rel} = A^{\rm rel}_{\rm max}/A^{\rm nr}_{\rm max}$ is the ratio of the maximum amplitudes of the relativistic $A^{\rm rel}_{\rm max}$ to the nonrelativistic $A^{\rm nr}_{\rm max}$ Compton peaks at $\theta_{\rm min}$. $\theta_{\rm min}$ is the smallest θ possible for the Compton peak maximum to be in the DDCS spectrum. $\theta_{n\%}$ is the largest θ in order to have an $n\%$ level of convergence of $\Delta\omega_2^{\rm rel}$. $\theta_{\rm max}$ is the θ at which $\Delta\omega_2^{\rm pk}$ is at its maximum.

ω_1 (keV)	Z	$\theta_{\rm min}$ (deg)	$\Delta\omega_2^{\rm rel}$ at $\theta_{\rm min}$	$R^{\rm rel}$ at $\theta_{\rm min}$	$\theta_{(0.1\%)}$ (deg)	$\theta_{(1\%)}$ (deg)	$\theta_{\rm max}$ (deg)
1000	15	2.8	8×10^{-6}	0.9921	10.6	19.6	68.5
1000	29	5.8	9.6×10^{-5}	0.9708	9.96	19.5	72.1
1000	62	13.0	2.05×10^{-3}	0.8699	–	20.1	82.1
1000	92	35.5	1.31×10^{-2}	0.7264	–	–	97.5
662	15	5.9	3.0×10^{-5}	0.9922	15.0	26.7	105.3
662	29	7.5	7.55×10^{-5}	0.9707	14.8	27.3	107.5
662	62	20.0	3.12×10^{-3}	0.8713	–	28.2	120.9
662	92	35.5	1.98×10^{-2}	0.7463	–	–	180
320	15	9.8	$5. \times 10^{-5}$	0.9921	24.5	51.1	180
320	29	17.8	2.25×10^{-5}	0.9708	25.8	51.1	180
320	62	45.0	7.53×10^{-3}	0.8937	–	49.9	180
320	92	103.0	4.41×10^{-2}	1.05	–	–	180

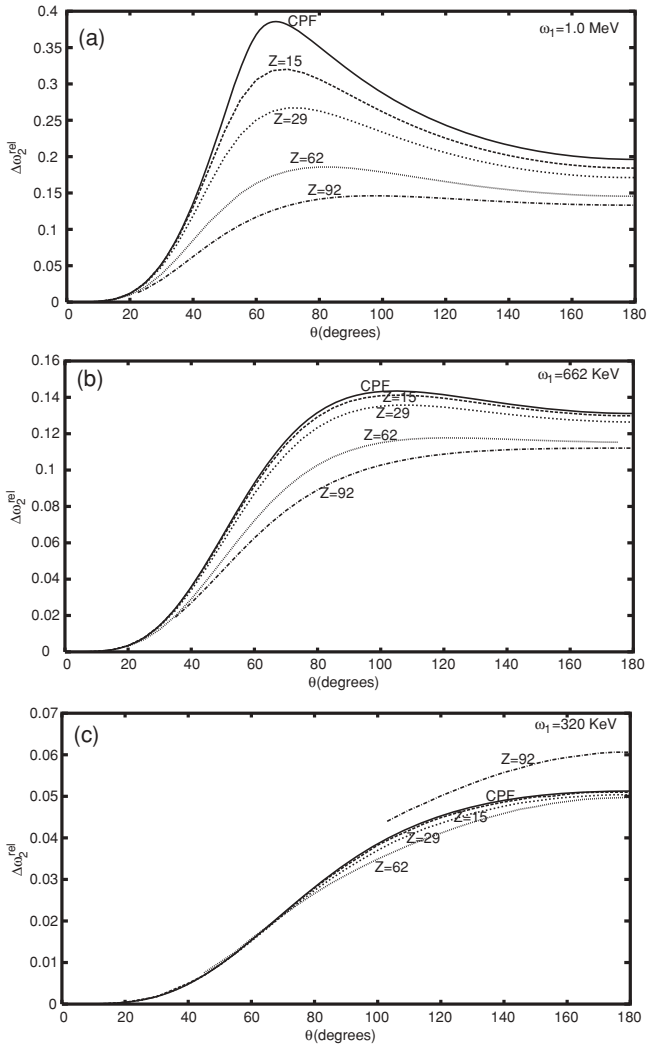

FIG. 4. θ, ω_1, and Z dependence of the relativistic shift $\Delta\omega_2^{\rm rel}$. The relativistic shift on the ω_1 scale is defined as $\Delta\omega_2^{\rm rel} = [{}^{\rm rel}\omega_2^{\rm pk} - {}^{\rm nr}\omega_2^{\rm pk}]/\omega_1$, where ${}^{\rm rel}\omega_2^{\rm pk}$ and ${}^{\rm nr}\omega_2^{\rm pk}$ are the ω_2 at which the RIA and NRIA Compton peaks have their maximum amplitude. CPF represents the relativistic shift of the Compton profile given by $\Delta\omega_2^{\rm rel} = [\omega_2(p_{\rm min} = 0) - \omega_2(p_z^{\rm nr} = 0)]/\omega_1$, where $\omega_2(p_{\rm min} = 0)$ and $\omega_2(p_z^{\rm nr} = 0)$ are given by Eqs. (11) and (12), respectively.

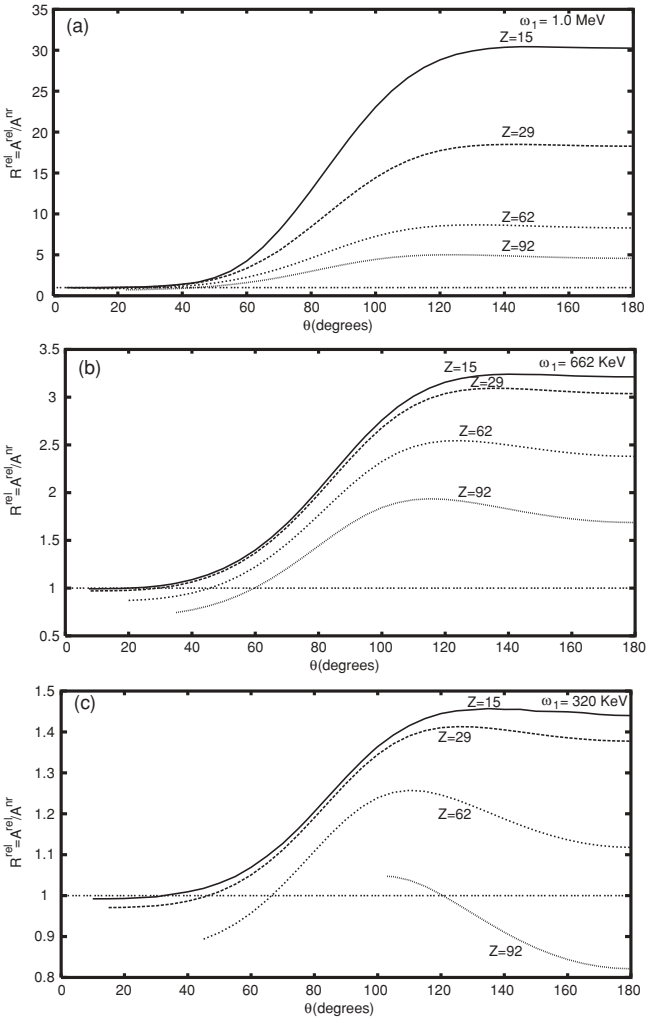

FIG. 5. θ, ω_1, and Z dependence of the relativistic increase in the Compton peak magnitude $R^{\rm rel}$. $R^{\rm rel} = A^{\rm rel}/A^{\rm nr}$, where $A^{\rm rel}$ and $A^{\rm nr}$ are the maximum amplitudes of the RIA and NRIA Compton peaks at ${}^{\rm rel}\omega_2^{\rm pk}$ and ${}^{\rm nr}\omega_2^{\rm pk}$, respectively.

Eq. (6)] as separable functions with respect to p rather than using the integrated full RIA expression [Eq. (5)]. Here the ρ factor is obtained from the difference between the maximum Compton peak amplitudes from Eqs. (5) versus (6), while the contribution from both the ρ and KJ factors comes from the corresponding difference in peak amplitudes from Eqs. (3) versus (5). Both the ρ and KJ factors cause $R_{\rm rel}$ to decrease with increasing Z. The contribution of the ρ factor is always proportional to Z^2 near the Compton profile maximum, but it is independent of ω_1 and θ, while the KJ factor, which is nearly independent of ω_1, is strongly dependent on θ, largest at 180°, and much smaller at small θ. For example, when $Z = 15$ and $\omega_1 = 662$ keV, the KJ factor causes a 1.2% increase in the Compton peak amplitude above its exact value when $\theta = 180°$ but only a 0.30% increase when $\theta = 5.9°$.

When $Z = 62$ the increase in peak magnitude is 19.0% and 5.2% when θ is 180° and 20°, respectively. The increase in the peak magnitude that results by replacing $\rho_{\rm rel}$ by $\rho_{\rm nr}$ is 0.50% and 9.5% when Z is 15 and 62, respectively. The increase of the KJ contribution is proportional to Z^2 at 180° and when θ is less than about 35°, but it deviates greatly from Z^2 behavior at intermediate angles. The Z^2 dependence of the KJ factor that results as $\theta \to 0°$ is because $\bar{X} \to X^{\rm nr} = 1 + \cos^2\theta$, causing $\bar{X}$ to become independent of p (see Fig. 1 and discussion in Sec. II B). Such effects will be explained in a future manuscript on a systematic comparison between Eqs. (5) and (6) with numerical examples and mathematical explanations for when and why Eq. (6) breaks down. The only factors that contribute significantly to the deviation of $R^{\rm rel}$ from unity at small θ are the ρ and KJ factors. Both effects are proportional to Z^2 and the KJ error is much smaller, in fact about one-fourth of what it is at $\theta = 180°$. Thus it should be easy to correct for any errors at small θ that would occur using nr expressions to calculate DDCS even when Z is fairly high.

IV. RELATIVISTIC CHARACTERIZATION OF THE A^2 MATRIX ELEMENT EXPRESSION FOR CALCULATING DDCS

The nonrelativistic first-order perturbation QED S-matrix expression for DDCS based on the first term of $H_{\rm int}$ designated by $\langle i|A^2|j\rangle$ (see Sec. I, can be made kinematically relativistic (see, for example, [4] and [8]) by making the momentum and energy of the ejected electron relativistic. In this section it is demonstrated that the relativistic shift of the Compton peak is associated with momentum, while the relativistic increase in the Compton peak amplitude is associated with energy. This separation of relativistic effects with respect to variables is similar to that in the corresponding RIA expression as discussed in Sec. III A. The main difference here is that, in the RIA expression, ρ is a separable factor which can be made relativistic or nonrelativistic, while in $\langle i|A^2|j\rangle$, the wave-function component which is nr cannot readily be factored out. Further, a modification of this approach for making the $\langle i|A^2|j\rangle$ expression for DDCS kinematically relativistic, which yields a more accurate Compton peak, will be proposed and tested.

The expression based on $\langle i|A^2|j\rangle$ for calculating DDCS is nonrelativistic but is derived from a more precise theory than the corresponding NRIA expression [Eq. (3)] and is given by

$$\frac{d^2\sigma}{d\omega_2 d\Omega_2} = r_0^2\left(\frac{\omega_2}{\omega_1}\right)\left(\frac{1+\cos^2\theta}{2}\right) \times \int_0^{\pi}\int_0^{2\pi} |\langle i|A^2|f\rangle|^2 \sin\theta_e d\theta_e d\phi_e, \quad (37)$$

where $\langle i|A^2|f\rangle$ [see Eq. (A2)] is derived from Eqs. (23) and (24) of Gavrila [21]. Here $\langle i|$ and $|f\rangle$ represent the initial and final states, respectively, and θ_e and ϕ_e are the polar and azimuthal angles for the ejected electron, respectively. His expression has been shown to yield an accurate Compton peak in nr regimes (see, for example, [14]). In Fig. 6, where $Z = 29$ and $\omega_1 = 320$ keV, peak 1 corresponds to the S-matrix, peak 2 to the RIA [Eq. (5)], and peak 3 to $\langle i|A^2|f\rangle$ predictions for DDCS. Peak 3 is shifted to a lower ω_2 by about 14 keV from peaks 1 and 2 and has a much smaller peak magnitude. If one replaces $p_f^{\rm nr}$ [Eq. (27)] by $p_f^{\rm rel}$ [Eq. (28)] in the $\langle i|A^2|f\rangle$ expression [Eq. (37)], the Compton peak shifts to higher ω_2, with a small increase in the peak magnitude due to the direct proportionality of DDCS to ω_2 [compare the Compton peak labeled 3 for $\langle i|A^2|f\rangle$ to that labeled 4 for $\langle i|A^2|f\rangle$ with $p_f^{\rm rel}$ in place of $p_f^{\rm nr}$ in Fig. 6]. This is similar to what would happen if one were to replace $p_z^{\rm nr}$ by $p_{\rm min}$ in J but not K using Eq. (6). If one replaces $E_f^{\rm nr}$ [Eq. (29)] by $E_f^{\rm rel}$ [Eq. (30)] with p_f still nr, the result is an increase in peak magnitude with no significant shift in the peak position (compare peak 5 to peak 3). Then $p_f^{\rm nr}$ and $E_f^{\rm nr}$ are replaced by $p_f^{\rm rel}$ and $E_f^{\rm rel}$, respectively. This modified matrix element is referred to as rpe$\langle i|A^2|f\rangle$ (where rpe stands for relativistic momentum and energy). By using rpe$\langle i|A^2|f\rangle$, the resulting peak 6 is in reasonable agreement with the S-matrix and RIA predictions, but it could be better. Apparently just making p_f and E_f relativistic is not quite enough. However, these results demonstrate that most of the relativistic shift is associated with $p_f^{\rm nr} \to p_f^{\rm rel}$ and the increase in the peak magnitude can be attributed to $E_f^{\rm nr} \to E_f^{\rm rel}$. The nr limit in this case occurs as $E_k \to 0$ rather than as $\theta \to 0$ as in the RIA case.

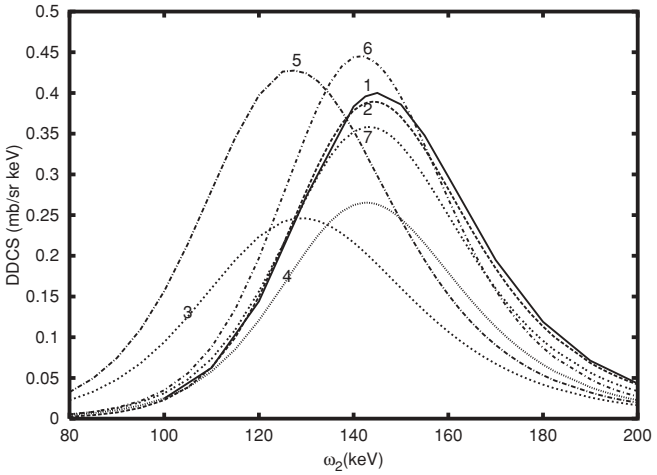

FIG. 6. Effect of relativistic kinematics on the prediction of the Compton peak for Cu (K-shell) calculated from modified and unmodified $\langle i|A^2|f\rangle$ [see Eq. (37) and the Appendix, Eq. (A2)] with $\omega_1 = 320$ keV and $\theta = 180^\circ$: $p_f^{\rm nr}$ [Eq. (27)]; $p_f^{\rm rel}$ [Eq. (28)]; $E_k^{\rm nr}$ [Eq. (29)]; $E_f^{\rm rel}$ [Eq. (30)]. 1, S-matrix, solid line; 2, RIA [Eq. (5)], short heavy dashes; 3, $\langle i|A^2|f\rangle$, heavy dots; 4, $\langle i|A^2|f\rangle$ with $p_f^{\rm rel}$ and $E_f^{\rm nr}$, fine dots; 5, $\langle i|A^2|f\rangle$ with $E_f^{\rm rel}$ and $p_f^{\rm nr}$, dots and long dashes; 6, $\langle i|A^2|f\rangle$ with $p_f^{\rm rel}$ and $E_f^{\rm rel}$ (rpe$\langle i|A^2|f\rangle$), dots and short dashes; 7, $\langle i|A^2|f\rangle$ with $p_f^{\rm rel}$ and $E_f^{\rm nr}$ and $X_{\rm nr} = 1+\cos^2\theta$ replaced by $\bar{X}(p_{\rm min})$ in Eq. (37) designated by $\bar{X}\langle i|A^2|f\rangle$.

One can obtain a more accurate Compton peak than peak 6 in Fig. 6, by replacing $1+\cos^2\theta = X^{\rm nr}$ in Eq. (37) by $\bar{X}(p_{\rm min})$ [Eqs. (13) and (18)], with $\langle i|A^2|f\rangle$ a function of $p_f^{\rm rel}$ and $E_f^{\rm nr}$. This modified expression for DDCS is referred to as $\bar{X}\langle i|A^2|f\rangle$. The idea here is that since the relativistic increase in the Compton peak magnitude is associated only with $E_f^{\rm nr} \to E_f^{\rm rel}$ (not $p_f^{\rm nr} \to p_f^{\rm rel}$) in $\langle i|A^2|f\rangle$ this effect is similar to the difference in the Compton peak magnitude predictions between $X^{\rm nr}$ and $\bar{X}$ in the RIA expression for DDCS. The resulting peak 7 has an $\omega_2^{\rm pk}$ that is in good agreement with peaks 1 and 2 and a magnitude that is just a little less than these two peaks.

In Figs. 7(a) and 7(b) for Cu with $\omega_1 = 662$ keV, the rpe$\langle i|A^2|f\rangle$ expression for DDCS yields a Compton peak magnitude that is over 75% greater than the S-matrix result when $\theta = 180^\circ$, while if $\theta = 120^\circ$ the difference decreases to about 45% (compare peak 3 for rpe$\langle i|A^2|f\rangle$ to peaks 1 and 2 for the S-matrix and RIA results, respectively). A large-θ and low-Z example was chosen because Costescu and Spanulescu [8] reported that, when $\omega_1 = 661$ keV, their expression can only yield a good Compton peak when $\theta \leqslant 60^\circ$. The other reason for this choice is that the contribution of the infrared rise to the Compton peak which is only due to the $\vec{p}\cdot\vec{A}$ matrix element ($\langle i|\vec{p}\cdot A|f\rangle$) is minimized when Z is low and tends to decrease with increasing θ. One apparent reason for the result of Costescu and Spanulescu [8] is that inelastic photon scattering behaves progressively less relativistic as $\theta \to 0^\circ$. Thus if ω_1 is not too relativistic, their approximation is good even at large θ, but as ω_1 is increased, θ must be progressively smaller such that the Compton peak behavior does not become

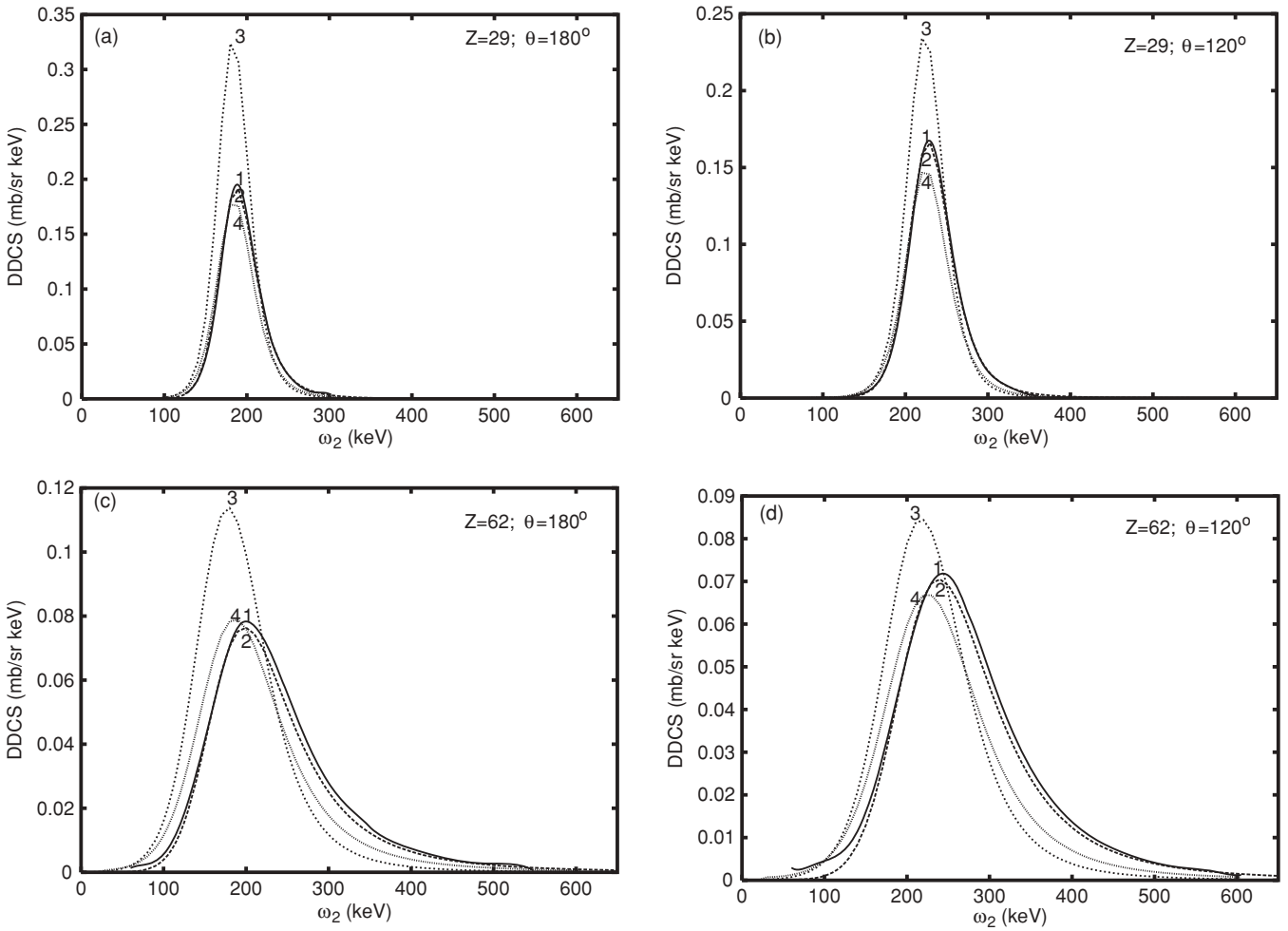

FIG. 7. Accuracy of K-shell DDCS obtained from $\bar{X}\langle i|A^2|f\rangle$ compared to rpe$\langle i|A^2|f\rangle$ at large θ with $\omega_1 = 662$ keV: 1, S-matrix, solid line; 2, RIA, short heavy dashes; 3, rpe$\langle i|A^2|f\rangle$, heavy dots; 4, $\bar{X}\langle i|A^2|f\rangle$, fine dots. (a) $Z = 29, \theta = 180^\circ$; (b) $Z = 29, \theta = 120^\circ$; (c) $Z = 62$, $\theta = 180^\circ$; (d) $Z = 62, \theta = 120^\circ$.

so relativistic that their approximation breaks down. The present results are much better when the Compton peak is obtained by using $\bar{X}\langle i|A^2|f\rangle$ rather than rpe$\langle i|A^2|f\rangle$ (compare peak 4 to peaks 1–3). The result is similar for Sm ($Z = 62$) with $\omega_1 = 662$ keV when $\theta = 180^\circ$ [Fig. 7(c)] and when $\theta = 120^\circ$ [Fig. 7(d)]. However, peak 4 is shifted to a slightly lower ω_2 compared to the RIA and S-matrix results (peaks 1 and 2). This shift becomes progressively more pronounced as Z is increased above $Z = 62$ (results of which are not shown). This shift to lower ω_2 is in part due to the difference in the respective nr limits for the $\langle i|A^2|f\rangle$ expression, which is $E_k \to 0$, and the corresponding RIA expression for DDCS, which is $\omega_2^{\rm pk} \to \omega_1$. This small shift, which might otherwise be larger, is probably reduced by the fact that there is no $\langle i|\vec{p}\cdot\vec{A}|f\rangle$ component included in the present calculations. This may also account for the fact that peak 4 in Figs. 7(c) and 7(d) is not greater in magnitude than peaks 1 and 2 even though at $Z = 62$ the magnitude of the nr Compton profile is almost 10% greater in magnitude than the relativistic one (see Sec. III B and Fig. 3). The magnitude of the $\bar{X}\langle i|A^2|f\rangle$ peak eventually does exceed that of the S-matrix and RIA results as Z is increased higher than 62 (also not shown). $\bar{X}\langle i|A^2|f\rangle$ always yields a more accurate Compton peak than rpe$\langle i|A^2|f\rangle$ when ω_1 is high, while the difference in the Compton peaks due to using $\bar{X}\langle i|A^2|f\rangle$ instead of rpe$\langle i|A^2|f\rangle$ decreases with decreasing ω_1. A more detailed study of the use of $\bar{X}\langle i|A^2|f\rangle$ for calculating both DDCS and TDCS will be given in a future paper. The use of a $\bar{X}\langle i|A^2|f\rangle$ expression should yield a more accurate Compton peak for TDCS (see the Appendix) than the corresponding RIA expressions. This is because IA theory breaks down for TDCS unless $\langle p_i\rangle/q \ll 1$, while for DDCS the requirement for accuracy is much less rigid and is $\langle p_i\rangle/q \leqslant 1$ [22]. Such limitations do not apply to the corresponding $\langle i|A^2|f\rangle$ expressions for DDCS or TDCS.

V. SUMMARY AND CONCLUSIONS

The low $q \to 0$ limit of the RIA expression for DDCS was taken in terms of ω_2 and θ, the differential variables for DDCS. This made it possible to characterize much of the relativistic kinematic contribution to DDCS as being due to the difference between $\omega_1\omega_2$ in $p_{\rm min}$ and $(\omega_1^2 + \omega_2^2)/2$ in $p_z^{\rm nr}$. This characterization was completed by linking $\omega_2^{\rm pk} \to \omega_1$ to the limit $p_{\rm min} \to p_z^{\rm nr}$ then to the relativistic shift of the Compton peak, which is due to the dependence of $J(p_{\rm min}, \rho)$ on $p_{\rm min}$, and to the relativistic increase in the peak magnitude due to

the dependence of $\bar{X}(p_{\min})$ on $p_{\min}$. The second limit $\theta \to 0$ leads to $\bar{X}(p_{\min}) \to 1 + \cos^2\theta \to 2$, which accounts for the remainder of the relativistic kinematic effect on the Compton peak, much of which also depends on the difference between one term in $p_{\min}$ and $p_z^{\rm nr}$. Also these two limits as well as $q \to 0$ are simultaneous at the Compton profile maximum where $p_{\min} = p_z^{\rm nr} = 0$. This characterization of relativistic contributions to the Compton peak provides a useful guide for estimating the relativistic effects under various circumstances and for knowing when purely nonrelativistic or kinamatically modified nr expressions will suffice at high energies. For example, this characterization shows that one can obtain accurate predictions for DDCS at any energy and scattering angle by using relativistic kinematics with a nonrelativistic charge density for atoms of nuclear charge less than about 30 (for K-shell ionization, or $E_b < 10$ keV in general). From the present results, one can also understand why good predictions for the position and magnitude of the Compton peak can be obtained from unmodified nonrelativistic expressions (not necessarily IA) even if $\omega > m$ if θ is small and $\langle p_i \rangle < m$ ($E_b < 10$ keV). In fact nr expressions can yield accurate predictions for the Compton peak even if v_e/c is as high as about 0.4. The θ range that would allow one to use nr expressions decreases with increasing ω_1. For example, at $\omega_1 = 3$ MeV, θ would have to be less than about 5° in order to obtain an accurate Compton peak; however, $\theta_{\min}$ also decreases with increasing ω_1.

Calculations from nr expressions generally do not require nearly as much computer resources as are needed for relativistic expressions. For example, calculation of DDCS using the relativistic code of Bergstrom [14] requires rapidly increasing amounts of computation time with increasing energy and decreasing binding energy of the ejected electron. Also computations when $\omega_1 > 900$ keV are not possible. If one is doing whole-atom DDCS calculations it is clearly not practical and sometimes not possible to use this fully relativistic code. Under such circumstances, it becomes necessary to use simpler nr expressions such as IA or if greater accuracy at small θ is needed one may use the nr S-matrix expressions of Gavrila [21], which provide accurate DDCS in nr regimes. Such expressions do not have the restrictions that the relativistic version does. Also any relativistic error due to $\rho_{\rm nr}$ is proportional to Z^2 near the Compton peak maximum and can be corrected. Thus knowing the ranges of θ, ω_1 and Z, over which nr expressions can be used helps one to choose the theoretical method that requires the least in computational resources (a big advantage for very large systems) but yields the necessary level of accuracy.

The present results indicate that it may be possible to use the simplest NRIA expression [Eq. (3)] even for a K-shell Compton peak for a fairly high Z at small θ, since the only significant relativistic effects that remain are those due to the ρ and KJ factors, both effects being proportional to Z^2. It should be possible to correct around the Compton peak maximum for Z at least as high as about 60 or $E_b < 50$ keV. For whole-atom DDCS, which are obtained from a weighted sum of subshell DDCS, one might use nr S-matrix expressions for the K and if necessary L shells, then use NRIA expressions for the remaining subshells at small θ. The simpler the expression the more possible it becomes to do calculations on larger systems such as whole atoms, molecules, and clusters as well as to make it easier to include electron-electron correlation effects in such larger systems.

The results given in Sec. IV show that one can use the improved kinematically relativistic $\langle i|A^2|f\rangle$ matrix element arrived at from the information gained in characterization of the RIA expression for DDCS to calculate DDCS, valid at any θ. If a more accurate Compton peak and/or a full DDCS spectrum is needed one may, in principle, combine $\langle i|A^2|f\rangle$ with a kinematically relativistic $\langle i|p\cdot A|f\rangle$.

ACKNOWLEDGMENTS

The author would like to thank Professor R. H. Pratt for the many helpful discussions on this topic. This work was supported by NSF Grant No. 0456499.

APPENDIX

The expression for triply differential cross sections, differential with respect to ω_2, the solid scattering angle Ω_2 of the photon, and the solid angle for the ejected electron Ω_e is given by

$$\frac{d^3\sigma}{d\omega_2 d\Omega_2 d\Omega_e} = r_0^2 \left(\frac{\omega_2}{\omega_1}\right)\left(\frac{1+\cos^2\theta}{2}\right)|\langle i|A^2|f\rangle|^2, \quad \text{(A1)}$$

where $\langle i|A^2|f\rangle$ is the A^2 matrix element, with $\langle i|$ and $|f\rangle$ representing the initial and final states, respectively. The explicit expression for the complex square of the $\langle i|A^2|f\rangle$ matrix element is given by

$$|\langle i|A^2|f\rangle|^2 = |N|^2 \frac{[q^2-(\vec{p}_f\cdot\vec{q})]^2 + \left(\frac{\alpha Z E_f}{p_f}\right)^2(\vec{p}_f\cdot\vec{q})^2]\exp\left[-2\left(\frac{\alpha Z E_f}{p_f}\right)\tan^{-1}\left(\frac{2\lambda p_f}{q^2 p_f^2+\lambda^2}\right)\right]}{\left[q^2\left(q^2-2p_f^2+2\lambda^2\right)+\left(\lambda^2+p_f^2\right)^2\right]\left[q^2+p_f^2+\lambda^2-2(\vec{q}\cdot\vec{p}_f)\right]^4}, \quad \text{(A2)}$$

where

$$\vec{p}_f\cdot\vec{q} = p_f[K_1\cos\theta_e - K_2(\sin\theta_e\cos\phi_e\sin\theta + \cos\theta_e\cos\theta)] \quad \text{(A3)}$$

and

$$N = \left(\frac{32}{\pi}\right)(2\lambda^5 pm)^{1/2}\exp\left(\pi\left|\frac{\alpha Z E_f}{i p_f}\right|/2\right)\Gamma\left(1-i\left|\frac{\alpha Z E_f}{i p_f}\right|\right). \quad \text{(A4)}$$

See Eqs. (27) or (28) for p_f; for $E_f = m + \omega_1 - \omega_2 - |E_b|$ see Eqs. (29) or (30) and $\lambda = \alpha Z m$.

[1] A. N. Hopersky and A. M. Nadolinsky, Phys. Rev. A **77**, 022712 (2008).
[2] J. Laukkanen, K. Hämäläinen, and Manninen, J. Phys: Condens. Matter **8**, 2153 (1996).
[3] S. Huotari, K. Hämäläinen, S. Manninen, S. Kaprzyk, A. Bansil, W. Caliebe, T. Buslaps, V. Honkimaki, and P. Suortti, Phys. Rev. B **62**, 7956 (2000).
[4] M. Schumacher, F. Smend, and I. Borchert, J. Phys. B **8**, 1428 (1975).
[5] F. Biggs, L. B. Mendelsohn, and J. B. Mann, At. Data Nucl. Data Tables **16**, 201 (1975).
[6] P. Holm and R. Ribberfors, Phys. Rev. A **40**, 6251 (1989).
[7] P. Eisenberger and P. M. Platzman, Phys. Rev. A **2**, 415 (1970).
[8] A. Costescu and S. Spanulescu, Phys. Rev. A **73**, 022702 (2006).
[9] R. Ribberfors, Phys. Rev. B **12**, 2067 (1975).
[10] J. M. Jauch and F. Rohrlich, *The Theory of Photons and Electrons* (Addison-Wesley, Cambridge, MA, 1955), pp. 163–169 and pp. 228–235.
[11] F. Bell, J. Phys. B **22**, 287 (1989).
[12] A. K. F. Haque, M. A. Uddin, A. K. Basak, K. R. Karim, B. C. Saha, and F. B. Malik, Phys. Lett. **354**, 449 (2006); A. K. F. Haque, M. A. Uddin, A. K. Basak, K. R. Karim, and B. C. Saha, Phys. Rev. A **73**, 012708 (2006); T. Kull and W. Nakel, J. Phys. B **30**, L815 (1997).
[13] V. D. Efros, W. Leidemann, G. Orlandini, and E. L. Tomusiak, Phys. Rev. C **72**, 011002(R) (2005); **69**, 044001 (2004).
[14] T. Suric, P. M. Bergstrom, K. Pisk, and R. H. Pratt, Phys. Rev. Lett. **67**, 189 (1991); P. M. Bergstrom, T. Suric, K. Pisk, and R. H. Pratt, Phys. Rev. A **48**, 1134 (1993).
[15] P. P. Kane, Radiat. Phys. Chem. **75**, 2195 (2006).
[16] M. Pradoux, H. Meunier, M. Avan, and G. Roche, Phys. Rev. A **16**, 2022 (1977).
[17] S. S. Gopal and B. Sanjeevaiah, J. Phys. B **13**, 273 (1980).
[18] W. C. Toye and P. N. Johnston, Appl. Rad. Isot. **49**, 815 (1998).
[19] P. Jaiswal and A. Shukla, Phys. Rev. A **75**, 022504 (2007).
[20] B. L. Abuja, M. Sharma, and H. Bross, Phys. Status Solidi B **244**, 642 (2007).
[21] M. Gavrilla, Phys. Rev. A **6**, 1348 (1972).
[22] Z. Kaliman, T. Suric, K. Pisk, and R. H. Pratt, Phys. Rev. A **57**, 2683 (1998).